SOLUTION MINING RESEARCH INSTITUTE
105 Apple Valley Circle
Clarks Summit, PA 18411, USA

Telephone: +1 570-585-8092
Fax: +1 570-585-8091
www.solutionmining.org

THERMO-MECHANICAL EFFECTS IN COMPRESSED AIR STORAGE (CAES)

Claire Lestringant, Ecole Polytechnique, Palaiseau, France
Pierre Bérest, Ecole Polytechnique, Palaiseau, France
Benoît Brouard, Brouard Consulting, Paris, France

SMRI Fall 2010 Technical Conference
4-5 October 2010
Leipzig, Germany

Solution Mining Research Institute Fall 2010 Technical Conference
Leipzig, Germany, 4-5 October 2010

THERMO-MECHANICAL EFFECTS IN A CAES

Claire Lestringant and Pierre Bérest, LMS, Ecole Polytechnique, France
Benoît Brouard, Brouard Consulting, Paris, France

SUMMARY

Various thermo-mechanical phenomena generated by high-frequency pressure cycles in a salt cavern are discussed. A simple analytical model proves that the depth of penetration of temperature changes is a small fraction of the radius of the cavern. However, temperature changes generate large thermal stresses. These phenomena are compared to several failure criteria (Ratigan et al.'s (1991) dilation criterion, DeVries et al.'s (2005) dilation criterion, no-tension and no-effective-tension criteria). In several cases, spalling at the cavern wall resulting from thermal stresses must be expected. A simplified solution has been developed to predict the long-term cavern-creep closure rate in an idealized spherical cavern when cavern pressure is cycled daily between an upper and lower bound.

INTRODUCTION

Natural gas caverns used to be operated on a seasonal basis: gas was injected in summer and withdrawn in winter, when demand is larger. Recently, new operating modes have been used in which caverns experience more than one cycle per year, and high withdrawal rates are required. The interest in Compressed Air Energy Storage (CAES) also has been increasing. This type of storage is characterized by greater pressure variation rates and daily or weekly cycles. From the perspective of rock mechanics, new and challenging problems must be addressed. On one hand, the specific effect of numerous cycles on rock strength (fatigue) must be examined, requiring laboratory investigation. On the other hand, because gas or air experiences large changes in temperature, not enough time is left between two cycles to reach equilibrium with rock mass temperature, causing significant thermal stresses to develop at the cavern wall, the standard stability criteria (onset of dilation, no-tension, no-effective-tension) must be revisited.

Several papers have been dedicated to this issue. Bauer and Sobolik (2009) analyzed stresses and closure rate in a CAES facility (air pressure cycled daily) and in a natural gas storage facility (gas pressure movements more frequent and erratic than in a conventional seasonal storage). Staudtmeister and Zapf (2010) analyzed the onset of dilatancy in a gas storage facility experiencing fast and frequent gas movement.

In this paper, the case of a daily-operated CAES facility is discussed. It is proved that daily evolutions of the stored air can be considered as almost adiabatic — i.e., air temperature changes are much larger than in a seasonal storage. Additional stresses generated by pressure and temperature changes during a cycle are discussed and compared to the Ratigan et al. (1991) dilation criterion, to the DeVries et al. (2005) dilation criterion and to the "no-effective-tension" criterion. A visco-plastic analysis also is performed. It is suggested that, after a great number of cycles, overall cavern behavior is the sum of a steady-state behavior plus a cyclic thermo-elastic behavior. The dilation criteria are discussed in this context.

1. AIR TEMPERATURE CHANGES

1.1. Adiabatic air-temperature changes during 1-day cycles

In a CAES facility, the cavern pressure is cycled daily, $P_a(t) = P_h + P_0 \cos \omega t$, $\omega = 2\pi/\tau$, $\tau = 1$ day. Air warms when its pressure increases and cools when its pressure decreases. However, heat exchange between cavern air and the rock mass restores thermal equilibrium. As a first approximation, the amount of air brought into (or withdrawn from) the cavern by the gas flowing into or from the cavern is neglected, and average air temperature, or T_h, is assumed to remain constant and equal to the rock temperature at cavern depth, or z: $T_h(°C) = 12°C + 0.03\ z$ (meters) is typical. These assumptions will be discussed in Section 1.3. When the cavern air temperature, or T_a, is assumed to be uniform, the following heat-exchange equations hold:

$$\left(\rho_a C_a^p \dot{T}_a + \frac{T_a}{\rho_a} \frac{\partial \rho_a}{\partial T}\bigg|_P \dot{P}_a \right) V = -\int_{\partial\Omega} K_{salt} \frac{\partial T_{salt}}{\partial n} da \tag{1}$$

$$\frac{\partial T_{salt}}{\partial t} = k_{salt} \Delta T_{salt} \tag{2}$$

$$P_a(t) = P_h + P_0 \cos \omega t \tag{3}$$

The first relation describes the first principle of thermodynamics applied to the cavern air mass; $\rho_a = \rho_a(P_a, T_a)$ is the state equation of air; the second relation is Fourier's equation for heat transfer in the rock mass; and $k_{salt} = K_{salt}/\rho_{salt} C_{salt}$ is the thermal diffusivity of rock salt. From dimensional analysis, two characteristic times can be inferred:

$$\begin{cases} t_c = \pi a^2 / k_{salt} \\ t_c' = t_c / \chi \end{cases}$$

where a is cavern radius and $\chi = \rho_{salt} C_{salt} / \rho_a C_a^p$. For instance V = 64,000 m^3, a = 25 m, $k_{salt} = 100$ m²/yr, $t_c = 4$ years, $\rho_a C_a^p = 50$ kJ/m^3-°C when air average pressure is $P_h = 5$ MPa, $\rho_{salt} C_{salt} = 2 \times 10^6$ J/m^3-°C and $t_c' = t_c/\chi \approx t_c/40$. Both t_c and t_c' are much longer than one day (the period of the pressure cycles) and, as a first approximation, heat transfer to the rock mass can be neglected. Note that this statement would be incorrect if the cavern were smaller or if the cycle period were longer than one day. Air transformations can be considered as adiabatic (i.e., no thermal exchange with the rock mass is considered), and

$$\rho_a C_a^p \dot{T}_a + \frac{T_a}{\rho_a} \frac{\partial \rho_a}{\partial T}\bigg|_P \dot{P}_a = 0 \tag{4}$$

When air is considered as a perfect gas, $P_a = \rho_a r T_a$, $C_a^p / C_a^v = \gamma \approx 1.4$ and $C_a^p - C_a^v = r$, and the adiabatic path is defined as

$$T_a(t)/T_a(0) = \left[P_a(t)/P_a(0) \right]^{\frac{\gamma-1}{\gamma}} \tag{5}$$

In the following, $P_a(t) = P_h + P_0 \cos \omega t$, and P_0 is relatively small when compared to P_h. A linearized expression can be accepted:

$$T_a(t) = T_h + \left(\frac{\gamma - 1}{\gamma}\right)\frac{T_h}{P_h} P_0 \cos \omega t = T_h + T_0 \cos \omega t \tag{6}$$

where $T_0 = (\gamma - 1) T_h \, P_0 / \gamma P_h$.

Temperature measurements performed in the Huntorf cavern (Quast, 1983) seem to confirm that temperature variations approximately are adiabatic. To check the validity of the "adiabatic" assumption, the set of heat transfer equations was solved, and it was verified that the flux of heat through the cavern walls remains smaller than 2% of the additional amount of heat in the cavern, vindicating the "adiabatic" assumption.

1.2. Changes in rock temperature

Even if heat exchanges with the rock mass could be neglected when the heat balance at cavern scale is considered, changes in air temperature generate some rock temperature changes at the cavern wall, and the following problem must be considered:

$$\frac{\partial T_{salt}}{\partial t} = k_{salt} \, \Delta T_{salt} \tag{7}$$

where $T_{salt} = T_a = T_h + T_0 \cos \omega t$ at the cavern wall, and $T_{salt} = T_h$ in the far field.

In the case of an idealized spherical cavern, the solution of this problem is

$$T_{salt}(r,t) = T_h + T_0 \frac{a}{r} \exp\left[-(r-a)\sqrt{\omega / 2k_{salt}}\right] \cos\left[\omega t - (r-a)\sqrt{\omega / 2k_{salt}}\right] \tag{8}$$

Typical temperature changes during a half-period are shown on Figure 1. This solution is governed by two characteristic times: $\tau = 2\pi/\omega$ is the period of the pressure variations; and $t_c = \pi a^2 / k_{salt}$ describes the heat-transfer rate in the cavern.

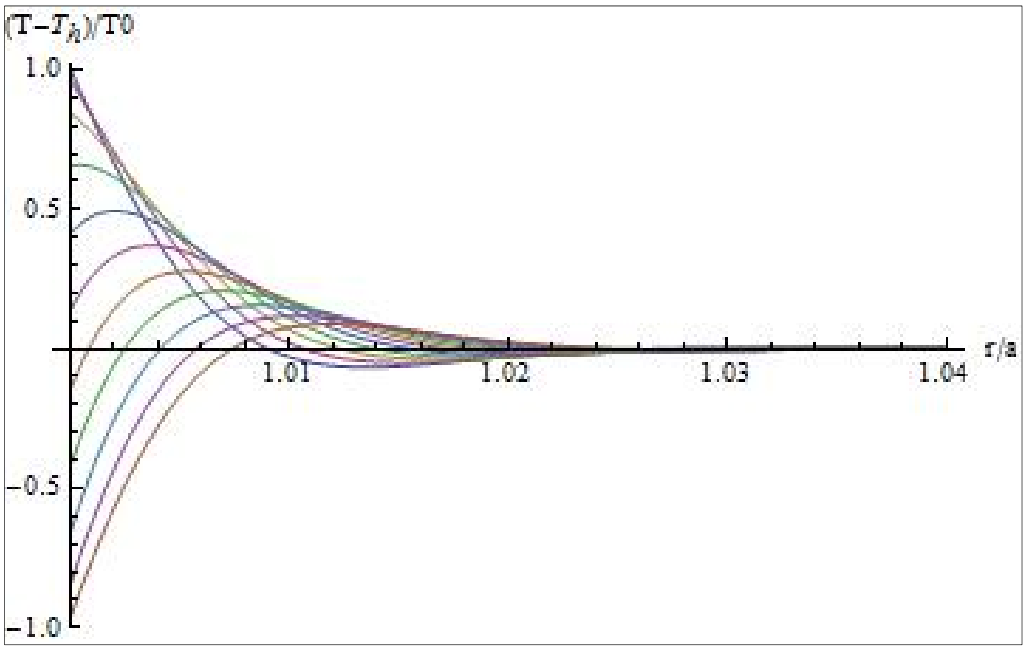

Figure 1. Temperature-change distribution in the rock mass as a function of radial distance to cavern center and time during a half-period. T_0 is the maximum cavern temperature change.

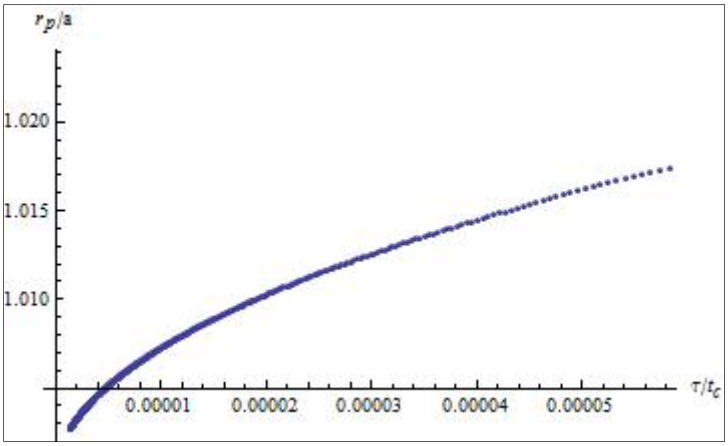

Figure 2. Relative depth of penetration (r_p/a) of thermal perturbations in the rock mass as a function of the ratio between the period of gas pressure variations (τ) and the characteristic time for heat transfer toward the rock mass (t_c). When considering a radius of *a* = 50 m, a time of $\tau = 1$ day, $\tau/t_c = 3.3\times10^{-5}$, and the thickness of the warmed salt layer at the cavern wall *is* $r_p - a = 65$ cm.

Let r_p be the depth of penetration of temperature changes — i.e., the distance from the cavern wall such that temperature changes are ten times smaller than temperature changes at the cavern wall, or $\frac{a}{r_p}\exp\left[-\left(r_p - a\right)\sqrt{\omega / 2k_{salt}}\right] = 0.1$ (Figure 2). In a 1,000,000-m^3 cavern, a = 50 m, τ =1 day, $k^p_{salt} = 100$ m²/yr and $\tau/t_c \approx 3.3\times10^{-5}$. In this case, the depth of penetration is $r_p/a = 1.013$, and only a thin layer of salt at the cavern wall experiences large changes in rock temperature. However, the additional stresses generated by the temperature changes cannot be neglected, as will be seen in Section 2.

1.3. Long-term evolution of cavern temperature

It was noted that during a brief cycle of change (1-day), heat exchange with the rock mass can be neglected, and gas transformation can be considered as almost perfectly adiabatic. However, when long-term evolutions are considered, heat transfer through the cavern walls can no longer be neglected. Furthermore, only a relatively small part of the air gas is injected/withdrawn during cavern operation, and the average temperature of the cavern gas slowly changes; thus, more refined computations are needed. In the following, we consider a 1500-m deep cavern with rock temperature at depth of 57 °C. In this example, cavern is created in one year, and the cavern brine temperature is assumed to be equal to injected brine temperature, or 12 °C. (This assumption is extremely pessimistic; in fact, cavern brine is warmer than 12 °C). When leaching is complete, the cavern air temperature is assumed to be 12 °C. Later, the gas pressure is cycled daily between $P_h - P_0 = 18 - 4.5$ MPa and $P_h + P_0 = 18 + 4.5$ MPa. The heat-exchange equation can be rewritten as

$$\left(\rho_a C_a^p \dot{T}_a + \frac{T_a}{\rho_a}\frac{\partial \rho_a}{\partial T}\bigg|_P \dot{P}_a\right) V = -\int_{\partial\Omega} K_{salt}\frac{\partial T_{salt}}{\partial n}da + q_m C_a^p \left(T_{inj} - T_a\right) \tag{9}$$

where q_m is the gas-mass flow rate into or from the cavern, and T_{inj} is the temperature of the gas injected in the cavern; the exact state equation of air is used. LOCAS software (Brouard et al., 2006) was used to solve this equation.

Results are presented in Figure 3. After the initial 1-year leaching phase, large daily fluctuations in gas temperature can be observed; however, the average gas temperature slowly increases and becomes progressively closer to the geothermal temperature.

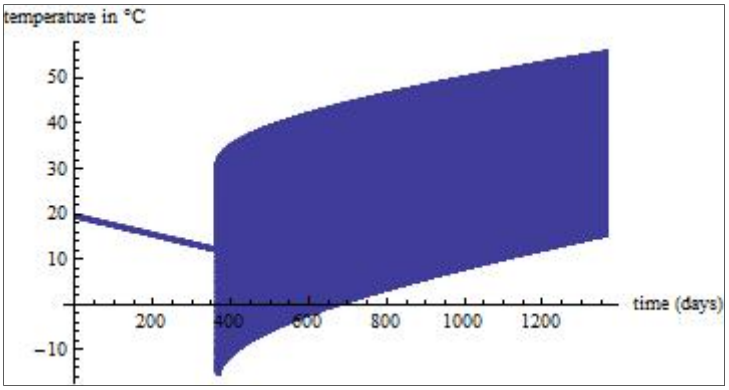

Figure 3 . Temperature evolution in a 1500-m deep cavern.

2. ADDITIONAL STRESSES GENERATED BY CHANGES IN ROCK TEMPERATURE

2.1. Additional stresses generated by temperature changes

In this section, we analyze the *additional* stresses generated by temperature changes. Obviously, in an actual cavern, these changes combine with stress changes generated by air pressure changes; these will be considered later. The system of equations to be solved in this situation is

$$\begin{cases} div\ \underline{\underline{\sigma}} = 0 \\ \underline{\underline{\varepsilon}} = \dfrac{1+\nu}{E}\underline{\underline{\sigma}} - \dfrac{\nu}{E}(tr\underline{\underline{\sigma}})\ \underline{\underline{1}} + \alpha_{salt}\, T_0 \cos\omega t\ \underline{\underline{1}} \\ \underline{\underline{\sigma}}.n = 0 \qquad \text{at cavern wall} \\ \sigma \to 0 \qquad \text{at large distances from the cavern} \end{cases} \tag{10}$$

where $\alpha_{salt} \approx 4\times10^{-5}/°\mathrm{C}$ is the thermal expansion coefficient of salt.

Spherical symmetry is assumed in the following, and the system can be rewritten as

$$\begin{cases} \partial\sigma_{rr}/\partial r + 2\left(\sigma_{rr} - \sigma_{\theta\theta}\right)/r = 0 \\ \varepsilon_{rr} = \dfrac{\partial u}{\partial r} = \dfrac{1}{E}\left(\sigma_{rr} - 2\nu\sigma_{\theta\theta}\right) + \alpha_{salt}\, T_0 \cos\omega t \\ \varepsilon_{\theta\theta} = \varepsilon_{\varphi\varphi} = \dfrac{u}{r} = \dfrac{1}{E}\left[\left(1-\nu\right)\sigma_{\theta\theta} - \nu\sigma_{rr}\right] + \alpha_{salt}\, T_0 \cos\omega t \\ \sigma_{rr}(a,t) = 0 \\ \sigma_{rr}(\infty,t) = 0 \end{cases} \tag{11}$$

The solution of this system can be written:

$$\begin{cases} \sigma_{rr}(r,t) = \Sigma\left[\cos\left(\omega t\right)h\left(r\right) + \sin\left(\omega t\right)g\left(r\right)\right] \\ h(r) = -u^3\sqrt{\dfrac{\tau}{t_c}} + \sqrt{\dfrac{\tau}{t_c}}u^2 exp\left[\sqrt{\dfrac{t_c}{\tau}}\left(1-\dfrac{1}{u}\right)\right]\left\{u^2\cos\left[\sqrt{\dfrac{t_c}{\tau}}\left(1-\dfrac{1}{u}\right)\right] - \sqrt{\dfrac{t_c}{\tau}}u^3\left(1+\sqrt{\dfrac{t_c}{\tau}}\dfrac{r}{a}\right)\sin\left[\sqrt{\dfrac{t_c}{\tau}}\left(1-\dfrac{1}{u}\right)\right]\right\} \\ g(r) = -\dfrac{\tau}{t_c}u^3\left(1+\sqrt{\dfrac{t_c}{\tau}}\right) + \sqrt{\dfrac{\tau}{t_c}}exp\left[\sqrt{\dfrac{t_c}{\tau}}\left(a-r\right)\right]\left\{u^2\sin\left[\sqrt{\dfrac{t_c}{\tau}}\left(1-\dfrac{1}{u}\right)\right] + \sqrt{\dfrac{\tau}{t_c}}u^3\left(1+\sqrt{\dfrac{t_c}{\tau}}\dfrac{1}{u}\right)\cos\left[\sqrt{\dfrac{\tau}{t_c}}\left(1-\dfrac{1}{u}\right)\right]\right\} \\ \sigma_{\theta\theta} = \sigma_{rr} + \dfrac{r}{2}\dfrac{\partial\sigma_{rr}}{\partial r} \\ u = a/r \end{cases} \tag{12}$$

The additional tangential stress at the cavern wall is especially large. It varies between $+\Sigma$ (a tensile additional stress reached when the gas temperature is lower, $T_a = T_h - T_0$) and $-\Sigma$ (a compressive additional stress reached when the gas temperature is higher, $T_a = T_h + T_0$), where

$$\Sigma = E\,\alpha_{salt}\,T_0 \big/ (1-\nu) \tag{13}$$

When $\nu = 0.25$, $E = 20$ GPa, $\alpha_{salt} = 4\times10^{-5}$/°C and $T_0 = 15$°C (a temperature change typically generated by a ± 1.5-MPa air-pressure change when the cavern depth is 725 m and the average air pressure is $P_h = 8.7$ MPa), $\Sigma = 17.3$ MPa — a large value. Radial and tangential stress distributions as a function of the distance to the cavern wall are represented in Figures 4a,b.

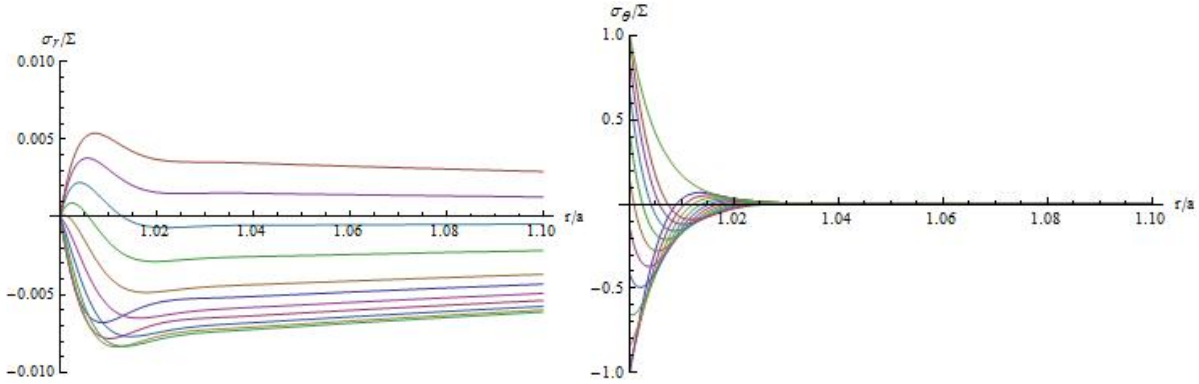

(a) **(b)**

Figures 4. Additional radial (a) and tangential stresses (b) divided by the maximum additional tangential stress ($\Sigma = 17.3$ MPa in the considered example) as a function of distance to the cavern center (r/a) and time during a half-cycle.

Additional radial stresses are small. The same cannot be said of additional tangential stresses, which are quite large in a narrow zone (width smaller than 3% of the cavern radius when the pressure-change period is one day). It can be expected that spalling will take place in this narrow zone. However, at this step, only *additional* stresses due to temperature changes were considered. A more general picture is obtained when stresses generated by pressure changes also are taken into account.

2.2. Additional stresses generated by temperature and pressure changes

We consider now the additional stresses generated by pressure changes. When the elastic behavior of a rock mass is assumed, the new problem is similar to the previous one. Equations are the same as those described in Section 2.2. In this case, however, $T_0 = 0$ (no temperature change), and the constitutive equations and boundary conditions can be written as:

$$\begin{cases} \sigma_{rr}(a,t) = -P_h - P_0\cos\omega t & \text{at cavern wall} \\ \sigma_{rr} \to -P_\infty & \text{at large distances from the cavern} \end{cases} \tag{14}$$

The solution of this problem is simple:

$$\begin{cases} \sigma_{rr}(r,t) = -P_\infty + \left(\dfrac{a}{r}\right)^3 \left(P_\infty - P_h - P_0\cos\omega t\right) \\ \sigma_{\theta\theta}(r,t) = -P_\infty - \dfrac{1}{2}\left(\dfrac{a}{r}\right)^3 \left(P_\infty - P_h - P_0\cos\omega t\right) \end{cases} \tag{15}$$

Because the thermo-elastic problem is linear, this solution simply can be added to the former solution to obtain the solution for the overall thermo-elastic problem: both pressure changes and the temperature changes generated by pressure changes are taken into account.

The tangential stress is of special interest. It varies between $-P_\infty - (P_\infty - P_h - P_0)/2 - \Sigma$ (reached when the gas pressure is higher, $P_a = P_h + P_0$) and $-P_\infty - (P_\infty - P_h + P_0)/2 + \Sigma$ (reached when the gas pressure is lower, $P_a = P_h - P_0$). We consider here the case of a 725-m-deep cavern and $P_h = 8.7$ MPa. Temperature changes are assumed to follow the "adiabatic" path. Gas pressure and temperature fluctuate between $P_h + P_0 = 10.2$ MPa, $T_h + T_0 = 48.75\,°C$ and $P_h - P_0 = 7.2$ MPa , $T_h - T_0 = 18.75\,°C$.

Figure 5a shows the tangential stresses; for ease of comparison, additional tangential stresses generated by temperature changes alone are provided in Figure 5b. Additional tangential stresses are modified (when compared to the case of temperature alone): they are lower, and additional compressive stresses are higher. Tensile stresses generated by low temperatures are somewhat lessened by compressive stresses generated by low pressures. The extent to which these stresses lead to damage in the salt wall is discussed in the next paragraph.

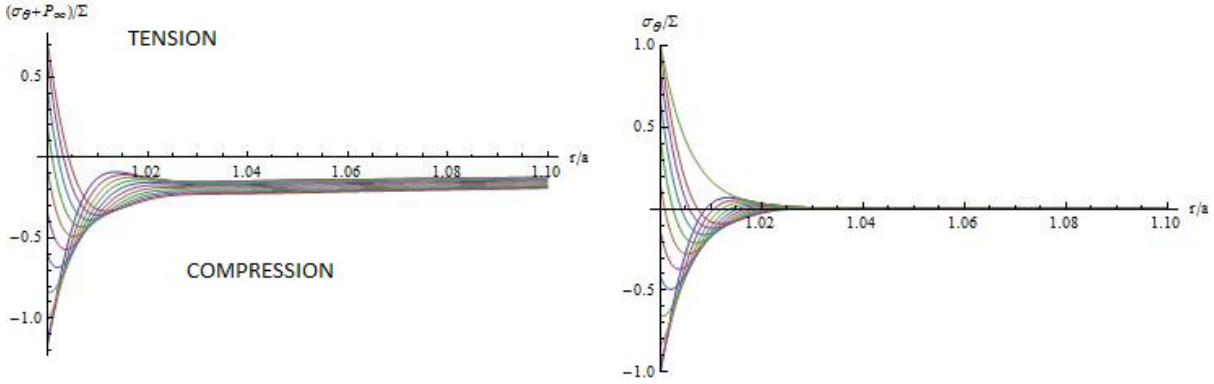

(a) **(b)**

Figure 5. Additional tangential stresses as a function of time when both pressure and temperature changes are taken into account (a) and when only temperature changes are taken into account (b).

2.3. Failure criteria

In the following, two families of failure criteria are discussed.

2.3.1. Dilation

When shear stresses are large (compared to the mean stress), salt micro-fracturing and dilation take place. These lead to porosity, an increase in permeability and a loss of rock strength. In the literature, the following two dilation criteria have been proposed.

- The Ratigan et al. (1991), Van Sambeek et al. (1993), VSR criterion is

$$\sqrt{J_2} < 0.27\,|I_1| \tag{16}$$

where $J_2 = s_{ij}s_{ji}/2$ is the second invariant of the deviatoric stress tensor, and $I_1 = \sigma_{kk}$ is the first invariant of the stress tensor. In the case of a spherical cavern, $3J_2 = (\sigma_{rr} - \sigma_{\theta\theta})^2$ and $I_1 = \sigma_{rr} + 2\sigma_{\theta\theta}$.

The VSR criterion does not take into account the three main components of the stress tensor. (At the cavern wall, the radial stress often is significantly less compressive than the two

tangential stresses, a situation opposite to the stress distribution in standard triaxial tests performed on rock samples.) Furthermore, it is overly pessimistic when mean stress is small.

- The DeVries et al. (2005) DV criterion suggests a more sophisticated formulation:

$$\sqrt{J_2} < \frac{D_1(|I_1|/\sigma_0)^m + \overline{T}_0}{\sqrt{3}\cos\psi - D_2\sin\psi} \tag{17}$$

where D_1, D_2, σ_0, $\overline{T}_0$ and m are five empirical constants, ψ is the Lode angle such that $\sin 3\psi = -3\sqrt{3}J_3/2J_2^{3/2}$, and $J_3 = s_{ij}s_{jk}s_{ki}/3$ is the third invariant of the deviatoric stress tensor. In the case of a spherical cavern, $J_3 = -2(\sigma_{rr} - \sigma_{\theta\theta})^3/27$ and ψ = -π/6 when $\sigma_{rr} - \sigma_{\theta\theta} < 0$ (an inequality that often holds for a cavern whose pressure is smaller than the overburden pressure).

  - In the so-called "extension case", the DV criterion is

$$\sqrt{J_2} < 2\left[D_1(|I_1|/\sigma_0)^m + \overline{T}_0\right]/(3 + D_2)$$

  - In the "compression" case, $\sigma_{rr} - \sigma_{\theta\theta} > 0$, $\psi = \pi/6$, and the DV criterion is written as

$$\sqrt{J_2} < 2\left[D_1(|I_1|/\sigma_0)^m + \overline{T}_0\right]/(3 - D_2)$$

  In the case of Cayuta (NY) salt, DeVries (2006) suggests the following parameter values: $D_1 = 0.733$ MPa, $D_2 = 0.52$, $\sigma_0 = 1$ MPa, $\overline{T}_0 = 1.95$ MPa, and $m = 0.69$.

2.3.2. Tension

When tensile stresses develop at the cavern wall, there is a risk of salt fracturing and spalling at the cavern wall. The following two criteria can be considered.

- No Tension — This criterion stipulates that no main stress must be tensile. In the context of a spherical cavern, the radial stress always is compressive. This criterion is written as

$$\sigma_{\theta\theta} < 0$$

- No Tensile Effective Stress at Cavern Wall: This criterion, suggested by Brouard et al. (2007), stipulates that the tangential compressive stress at the cavern wall must be smaller than the cavern fluid pressure, or

$$\sigma_{\theta\theta} + P < 0$$

  When this criterion is not met, there is a risk that hydro-fracturing takes place. This criterion is much more demanding than the "No-tension" criterion. It is not met when a gas-filled cavern is submitted to a fast and large pressure increase. It must be noted that this criterion is of purely theoretical origin; whether it actually applies to a real salt cavern has not yet been investigated fully.

2.4. Example

Here, again, the case of a 725-m-deep cavern is considered: the average gas pressure is P_h = 8.7 MPa; and the pressure and temperature changes are linked through the "adiabatic" relation, $T_0 = (\gamma - 1)T_hP_0/\gamma P_h$. The criteria are discussed in the most severe cases — i.e., when air pressure is

maximum or minimum. Figures 6, 7 and 8 display the dilatancy (VSR), no-tension and no-effective-tension criteria in the pressure-cycle-amplitude versus temperature-cycle-amplitude plane. The dilation criterion is especially demanding when temperature and pressure are high; the opposite is true when the effective stress criterion is considered. In fact, the no-effective-tension criterion is by far the more demanding.

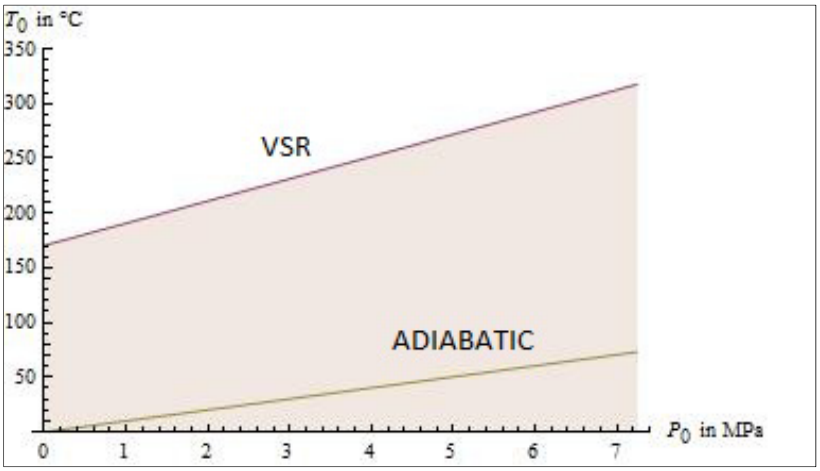

Figure 6. In the colored zone of the pressure-cycle-amplitude versus temperature-cycle-amplitude plane, the VSR dilation criterion is met. The "adiabatic" path is the path effectively followed by pressure and temperature during a cycle.

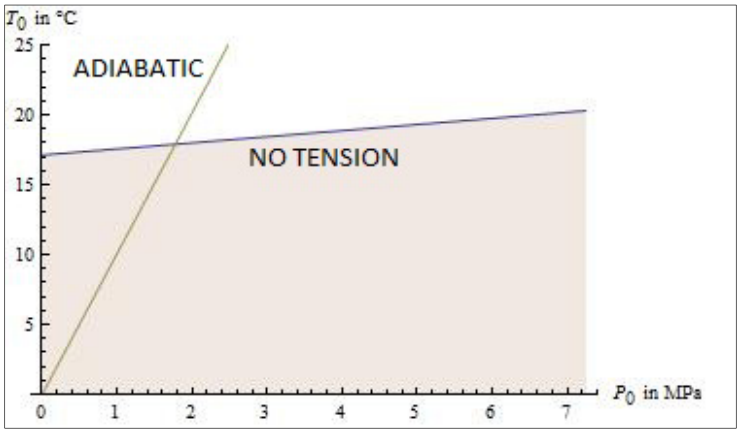

Figure 7. In the colored zone, the no-effective-tension criterion is met (same example as Figure 8). The dotted line is the "adiabatic" path. This criterion is much more demanding than the no-dilation criterion.

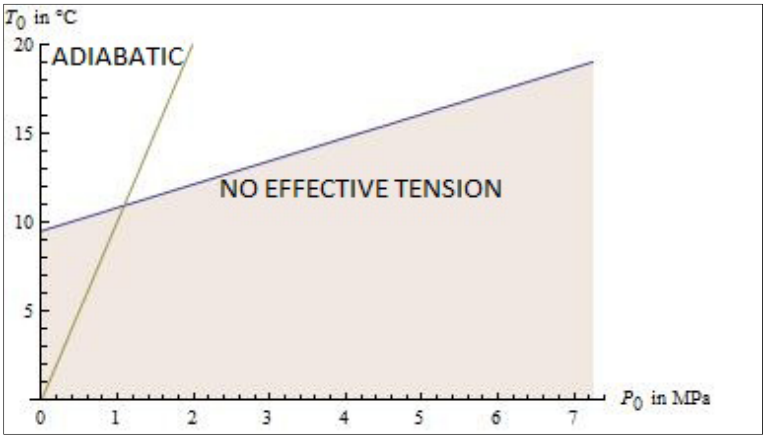

Figure 8. In the colored zone, the no-effective tension criterion is met (same example as Figure 8). The criterion is violated when cavern pressure (and temperature) are high. This criterion is more demanding than the no-dilation criterion.

2.5. Factor of safety

For the two dilation criteria (VSR and DV), a factor of safety (FS) is defined (see Figure 9; FS = OB/OA). A state of stress ($|I_1|, \sqrt{J_2}$) is safe when FS < 1.

When the VSR dilation criterion is considered, FS is smaller than 1 (Figure 10a). The same example as in 2.4 is considered. When the "extensive" DV criterion is considered, FS is larger than 1 in a small layer at the cavern wall (Figure 10b).

In conclusion, during a pressure cycle, both the no-effective-tension criterion and the DV-extension criterion are violated in a thin layer at the cavern wall, leading to cavern spalling. This effect is more pronounced in a deeper cavern and when pressure cycles are larger.

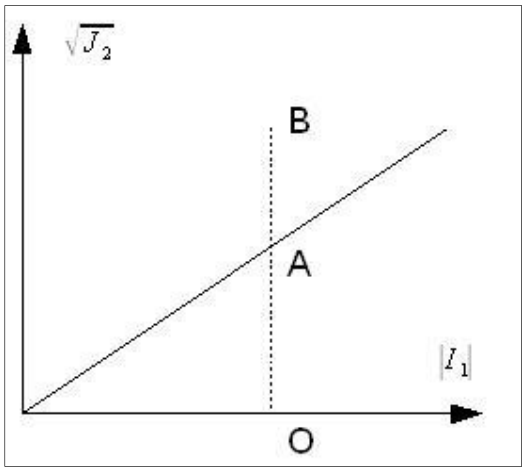

Figure 9. Factor of safety.

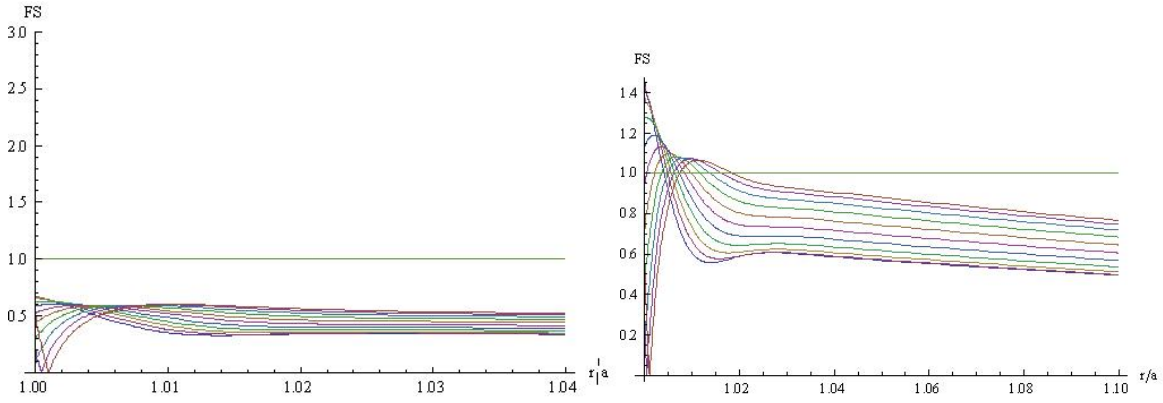

(a) **(b)**

Figure 10, Factor of safety as a function of the distance to the cavern center at different times during a half-period (same example as before): (a) VSR criterion and (b) DV-extension.-

3. VISCOPLASTIC BEHAVIOR

3.1. Asymptotic solution

In the former paragraphs, thermo-elastic behavior of the rock mass was assumed. In this section, the visco-plastic behavior of rock salt is taken into account. A simplified constitutive behavior is considered: $\dot{\varepsilon} = A^* \sigma^n$. It is assumed that the overall behavior of the cavern is the sum of cyclic, elastic (or thermo-elastic) behavior plus steady-state Norton-Hoff visco-plastic behavior. The exponent of the power law is $n = 3$, and the Poisson's ratio is $\nu = 0.5$ (no elastic volume change). The steady-state visco-plastic behavior is influenced by the average effect of the daily cycles. Computations are

detailed in the Appendix. This solution cannot be considered as exact, from a mathematical point of view, but it provides a first approximation of the effects of the cycles.

An example is provided in Figure 11. A 725-m-deep cavern is considered. Temperature effects are not taken into account at this step. The upper curve represents the yearly volume loss rate as a function of caver n pressure when a steady state is reached. This rate is zero when the cavern pressure equals the geostatic pressure ($P_a = P_\infty = 15.9$ MPa). When cavern pressure is zero, the volume loss rate is slightly slower than 7×10^{-3} /yr. The blue curve is interpreted as follows, assuming cyclic loading: the average gas pressure is $P_h = 8.7$ MPa the cycle amplitude is $P_0 = 3.7$ MPa , and the cavern pressure varies between $P_h - P_0 = 5$ MPa and $P_h + P_0 = 12.4$ MPa.

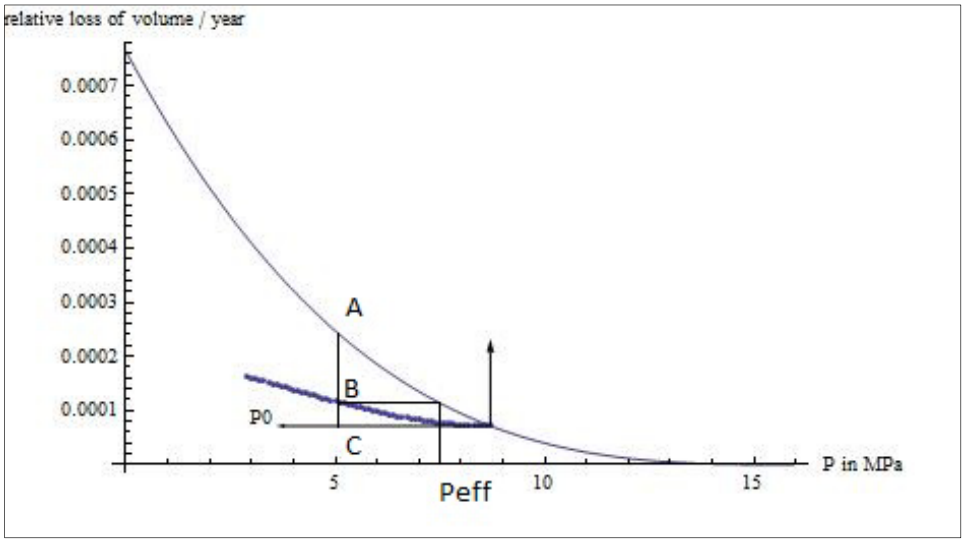

Figure 11. Volume loss rate as a function of gas pressure and gas-pressure changes. Average cavern depth is 725 m, and cavern pressure is cycled between 5 MPa and 12.4 MPa. P_{eff} is the (constant) cavern pressure for which the steady-state creep rate is the same as the average rate when the gas pressure is cycled between 5 MPa and 12.4 MPa

Point A (respectively, C) provides the steady-state volume-loss rate when the cavern pressure is kept constant and equal to the minimum pressure, $P_a = 5$ MPa (respectively, equal to the average pressure, $P_h = 8.7$ MPa). Point B provides the average steady-state volume rate observed when the cavern pressure is cycled between 5 MPa and 12.4 MPa. As expected, this average steady-state volume rate is slower than the steady-state volume loss rate when cavern pressure is lowest (A); it is faster than the steady-state volume loss rate when cavern pressure is kept constant and equal to the average gas pressure (C) because the constitutive law is non-linear.

In the former paragraph, thermo-elastic effects were not considered. In Figure 12, the relative volume loss rate of a 725-m-deep cavern as a function of cycle amplitude (P_0) is represented (average pressure during a cycle is $P_h = 8.7$ MPa). The lower curve corresponds to the case when no thermal effect is considered; the upper curve corresponds to the case when it is assumed that pressure cycles generate temperature cycles according to the “adiabatic” path. The steady-state volume-loss rate is faster when thermo-mechanical effects are taken into account.

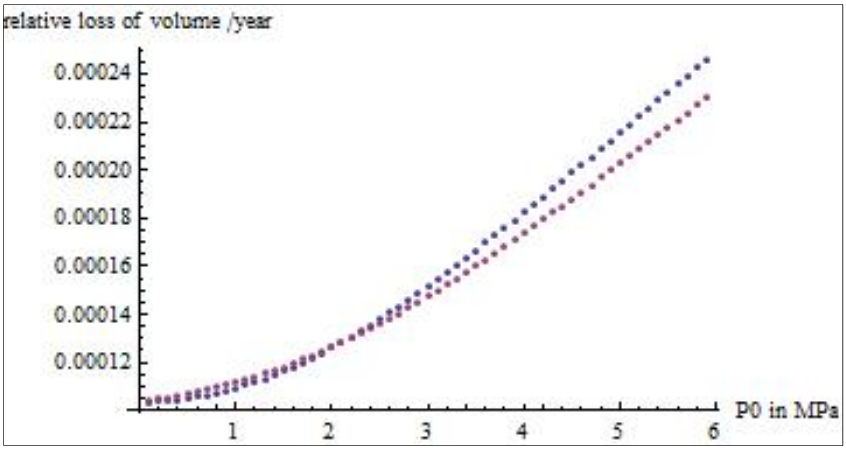

Figure 15. Relative steady-state volume-loss rate when thermal effects are taken into account (upper curve) and when they are not (lower curve).

3.2. Dilation criteria

In the $|I_1|,\sqrt{J_2}$ plane (the "invariant" plane also considered by Staudtmeister and Zapf, 2010), the VSR dilation criterion ($\sqrt{J_2}=0.27|I_1|$) is represented by a straight line (Figure 12). The DV criteria are represented by two parabola-like curves. The upper curve is associated with a "compressive" state of stress ($\sigma_{\theta\theta}=\sigma_{\varphi\varphi}>\sigma_{rr}$); the lower curve is associated with an "extensive" state of stress $\sigma_{rr}>\sigma_{\theta\theta}=\sigma_{\varphi\varphi}$.

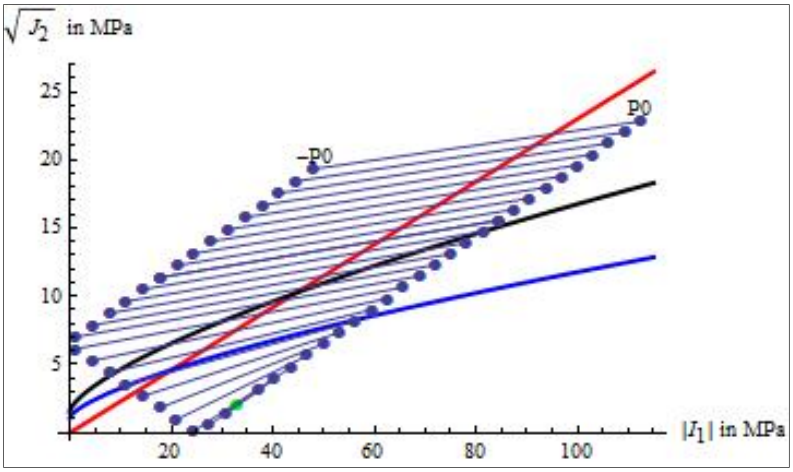

Figure 12. Stress paths in the « invariant » plane $\left(|I_1|,\sqrt{J_2}\right)$. Cavern depth is 725 m, and the average air pressure is 8.7 MPa. The VSR criterion, DV-extension criterion and DV-compression criterion are represented. Each segment represents the path followed by $\left(|I_1|,\sqrt{J_2}\right)$ when pressure is cycled between P_h-P_0 and P_h+P_0. Different values of the amplitude of the pressure changes, from $P_0=0.1$ MPa to $P_0=2.5$ MPa, are represented.

The cavern is 725-m deep, and the average gas pressure is $P_h=8.7$ MPa. Fifteen different values of P_0, the amplitude of the gas pressure cycles, are considered from $P_0=0.1$ MPa and $P_0=1.5$ MPa. For each of these values, values of $|I_1|$ and $\sqrt{J_2}$ during a cycle are drawn. (The representative points move along a straight line.) As soon as $P_0>0.7$ MPa, the (extension) DV criterion is violated. It can be

observed that the VSR criterion was never violated when a thermo-elastic analysis was performed. When visco-plastic effects are taken into account, it is violated as soon as $P_0 > 0.6$ MPa.

4. CONCLUSIONS

The main conclusions of this study are as follows.

- Daily pressure cycles generate *adiabatic* temperature changes.
- Pressure-temperature changes during a daily cycle generate large stresses in a thin layer at the cavern wall. Dilation and tension are likely to occur, leading to rock spalling at the cavern wall.
- A simplified steady-state visco-plastic solution is proposed. It proves that the steady-state cavern closure rate is slower in a CAES facility than it is in a cavern whose pressure is kept constant and equal to the minimum pressure applied during a cycle. An "effective (constant) pressure" can be defined such that steady-state volume-loss rate generated by this pressure is the same as the average volume-loss rate generated by a cyclic pressure.
- Numerical solutions raise a difficult problem, as the cycle period is much shorter than the period of time of interest (several decades) and thermal stresses are large in a very small domain at the cavern wall.

REFERENCES

Bauer S. and Sobolik S. (2009) Pressure cycling in compressed Air and Natural Gas Storage Caverns in Salt: Tracking Stress States and Cavern Closure Using 3-D Finite Element Analysis. SMRI Spring Meeting, Krakow, Poland, p.129.

Brouard B., Bérest P. and Karimi-Jafari M. (2007) Onset of Tensile Effective Stresses in Gas Storage Caverns. SMRI Fall Meeting, Halifax, p.119-135.

Brouard B., Karimi-Jafari M., Bérest P. and Frangi A. Using LOCAS Software to Better Understand the Behavior of Salt Caverns. Proc. SMRI Spring Meeting, Brussels, p. 273-288.

DeVries K.L. (2006) Geomechanical Analyses to Determine the Onset of Dilation around Natural Gas Storage Caverns in Bedded Salt. Proc. SMRI Spring Meeting, Brussels, p.131-150.

DeVries K.L., Mellegard K.D., Callahan G.D. and Goodman W.M. (2005) Cavern Roof Stability for Natural Gas Storage in Bedded Salt. Report RSI-1829, prepared by RE/SPEC Inc., Rapid City, SD, for United States Department of Energy, National Energy Technology Laboratory, Pittsburgh, PA.

Quast P. (1983). Plus de trois années de fonctionnement de cavités à air comprimé (More Than Three Years of CAES Operating Experience), in French. Annales des Mines, n° 5-6, 1983, p. 93-102.

Ratigan J.L., Van Sambeek L.L., DeVries K.L. and Nieland J.D. (1991) The Influence of Seal Design on the Development of the Disturbed Rock Zone in the WIPP Alcove Seal Tests. Report RSI-0400, prepared by RE/SPEC Inc., Rapid City, SD, for Sandia National Laboratories, Albuquerque, NM.

Staudtmeister K. and Zapf D. (2010). Rock Mechanical Design of Gas Storage Caverns for Seasonal Storage and Cyclic Operations. SMRI Spring Meeting, Grand Junction, Co, p.197-213.

Van Sambeek L.L., Ratigan J.L. and Hansen F.D. (1993) Dilatancy of Rock Salt in Laboratory Test. Proc. 34th US Symp. On Rock Mechanics, University of Wisconsin-Madison, WI, June 27-30, B.C. Haimson (ed.), Int. J. Rock Mech. Min. Sci. & Geomech. Abs., ***30***(7), 735-738.

APPENDIX

An idealized spherical cavern is considered. Cavern pressure is cycled between $P_h - P_0$ and $P_h + P_0$. The cycle period is $\tau = 2\pi/\omega$. Mechanical evolutions can be described by the following set of equations:

$$\frac{\partial \sigma_{rr}}{\partial r} + \frac{2(\sigma_{rr} - \sigma_{\theta\theta})}{r} = 0 \tag{18}$$

$$\dot{\varepsilon}_{rr} = \frac{\partial \dot{u}}{\partial r} = \frac{1}{E}\left(\dot{\sigma}_{rr} - 2\nu\dot{\sigma}_{\theta\theta}\right) + A^*\left(\sigma_{rr} - \sigma_{\theta\theta}\right)^n \tag{19}$$

$$\dot{\varepsilon}_{\theta\theta} = \dot{\varepsilon}_{\varphi\varphi} = \frac{\dot{u}}{r} = \frac{1}{E}\left[\left(1-\nu\right)\dot{\sigma}_{\theta\theta} - \nu\dot{\sigma}_{rr}\right] - \frac{A^*}{2}\left(\sigma_{rr} - \sigma_{\theta\theta}\right)^n \tag{20}$$

$$\sigma_{rr}(a, t > 0) = -P_h + P_0 \sin \omega t \tag{21}$$

$$\sigma_{rr}(\infty, t) = -P_\infty \tag{22}$$

Equation (18) illustrates the equilibrium condition; (19) and (20) describe the visco-plastic behavior of the rock mass; (21) is the boundary condition at the cavern wall; and (22) is the boundary condition at a large distance from the cavern. It is assumed that, in the long term, the overall cavern behavior can be considered as the sum of an instantaneous elastic behavior (as described in Section 2.2) plus an average "steady-state" behavior:

$$\sigma_{rr}(r,t) = \bar{\sigma}_{rr}(r) + P_0\left(\frac{a}{r}\right)^3 \sin \omega t \tag{23}$$

$$\sigma_{\theta\theta}\left(r,t\right) = \bar{\sigma}_{\theta\theta}\left(r\right) - \frac{P_0}{2}\left(\frac{a}{r}\right)^3 \sin \omega t \tag{24}$$

$$u_{rr}\left(r,t\right) = \bar{u}_{rr}\left(r\right) + \frac{3\left(1+\nu\right)P_0}{2E}\frac{a^3}{r^2}\sin \omega t \tag{25}$$

$$\dot{a}(t) = \dot{\bar{a}} + \frac{3(1+\nu)P_0}{2E}\omega \cos \omega t \tag{26}$$

When the Poisson's ratio is taken as $\nu = 0.5,$ no volume change takes place, and $\dot{u} = a^2\dot{a}/r^3$; Equation (20) takes the more simple form:

$$\frac{a^2\dot{a}}{r^3} = \frac{r}{2E}\frac{\partial \sigma_r}{\partial t \partial r} - \frac{A^*}{2}\left(-\frac{r}{2}\frac{\partial \sigma_r}{\partial r}\right)^n \tag{27}$$

$$-\frac{r}{2}\frac{\partial \sigma_r}{\partial r} = -\sigma_\theta + \sigma_r = f(r) + \frac{3}{2}\left(\frac{a}{r}\right)^3 P_0 \sin\left(\frac{2\pi}{T}t\right) \tag{28}$$

where $f(r) = -\frac{r}{2}\frac{\partial \bar{\sigma}_r}{\partial r}$ is the average value of $-\sigma_\theta + \sigma_r$ during one period, and

$$\frac{a^2 \dot{a}}{r^4} = \frac{1}{2E}\frac{\partial \sigma_r}{\partial t \partial r} - \frac{A^*}{2r}\left[f(r) + \frac{3}{2}\left(\frac{a}{r}\right)^3 P_0 \sin\left(\frac{2\pi}{T}t\right)\right]^n \tag{28}$$

Now, the following relation is integrated on one period, $\tau = 2\pi/\omega$:

$$\frac{a^2 \overline{\dot{a}}}{r^4} = -\frac{1}{\tau}\int_t^{t+\tau} \left\{ \frac{A^*}{2r}\left[f(r) + \frac{3}{2}\left(\frac{a}{r}\right)^3 P_0 \sin\left(\frac{2\pi}{\tau}t\right)\right]^n \right\} dt \tag{29}$$

When, for instance, $n = 3$, this relation is written as

$$\frac{a^2 \overline{\dot{a}}}{r^4} = -\frac{A^*}{2r}\left[f(r)^3 + \frac{9}{4} f(r)\left(\frac{a}{r}\right)^6 P_0^{\,2}\right] \tag{30}$$

This algebraic equation can be solved numerically, and the equilibrium equation $\partial \bar{\sigma}_r / \partial r = -2 f(r)/r$ can be integrated between $r = a$ and $r = \infty$.